

Cultivating $|T\rangle$ states on the surface code with only two-qubit gates

Jahan Claes*

Logiqal Inc., Monmouth Junction, NJ 08852, USA

High-fidelity $|T\rangle$ magic states are a key requirement for fault-tolerant quantum computing in 2D. It has generally been assumed that preparing high-fidelity $|T\rangle$ states requires noisy injection of $|T\rangle$ states followed by lengthy distillation routines. This assumption has been recently challenged by the introduction of *cultivation*, in which careful state injection and postselection alone are used to prepare $|T\rangle$ states close to the fidelity required for quantum algorithms. Cultivation was originally proposed for the color code [1], but can also be done on the \mathbb{RP}^2 code [2], a code similar to the surface code.

In this work, we demonstrate how to cultivate $|T\rangle$ states directly on the surface code. Besides its simplicity compared to color or \mathbb{RP}^2 cultivation, surface code cultivation offers a number of advantages, including: (1) It is more directly compatible with neutral atom architectures than \mathbb{RP}^2 cultivation (2) Cultivated surface code states can be used in transversal CNOT gates with other surface codes, unlike color code states (3) Surface code cultivation can be done at any distance, unlike color and \mathbb{RP}^2 cultivation which requires odd distances. Under a standard depolarizing error model, our $d = 3$ ($d = 4$) ($d = 5$) cultivation reaches an error rate of $1 \cdot 10^{-6}$ ($1 \cdot 10^{-8}$) ($2 \cdot 10^{-9}$) and an acceptance rate of 34% (6%) (1%), meeting or exceeding the fidelity of color and \mathbb{RP}^2 cultivation with comparable acceptance rates.

I. INTRODUCTION

Fault-tolerant quantum computation in 2D requires preparing high-fidelity *magic states*, non-stabilizer states that can be used to teleport non-Clifford gates [3–6]. Historically, it was believed that preparing magic states required a two-step process: first, noisy magic states would be injected into the error-correcting code [7]; second, many noisy magic states would be distilled into a single high-fidelity magic state using protected Clifford operations [4, 8, 9]. However, it has recently been proposed that a more involved injection procedure using repeated error checks and postselection can generate much higher-fidelity $|T\rangle := |0\rangle + e^{i\pi/4}|1\rangle$ magic states than previously thought possible, reducing or potentially eliminating the need for distillation. This postselection procedure is known as *cultivation* [1].

In the original cultivation proposal [1], as well as in earlier precursors to cultivation [10, 11], the authors injected $|T\rangle$ states into the color code [12]. The color code possesses a transversal $H_{XY} := (X + Y)/\sqrt{2}$ gate, allowing for double-checking the $|T\rangle$ state by fault-tolerantly measuring the logical H_{XY} operator ($|T\rangle$ is the +1 eigenstate of H_{XY} , so measuring logical H_{XY} checks that the logical state is correct). However, cultivating in the color code is not ideal, as many proposals for fault-tolerant quantum computing are based on the surface code [13–19], which is easier to implement and decode. Ref [1] address this by grafting their cultivated color code into a larger matchable code with two surface-code-like boundaries capable of performing lattice surgery with other surface code qubits. However, the grafted code is somewhat unwieldy. It is not directly usable in architectures that

use transversal CNOTs rather than lattice surgery, such as neutral atoms. It was also noted in Ref. [1, Fig. 16] that the grafted code has a higher error rate than the surface code. It would thus be desirable to cultivate directly on the surface code.

Two recent proposals have made partial progress in surface code cultivation. Both of these proposals are tailored to neutral atoms, requiring the flexible connectivity enabled by reconfigurable qubits. First, Ref. [20] proposed a method for cultivating two-qubit $|CX\rangle$ magic states on two patches of surface code. However, this method has three drawbacks: (1) it uses physical three-qubit CCX gates, which are more difficult to implement than two-qubit gates; (2) $|CX\rangle$ states cannot be used directly to teleport gates, but must be probabilistically converted into Toffoli states [21, 22]; (3) it produces $|CX\rangle$ states that are roughly $10^3 \times$ noisier than the $|T\rangle$ states produced by color code cultivation. Second, Ref. [2] proposed a method for cultivating $|T\rangle$ states on a variant of the surface code using only two-qubit gates; this method achieves similar fidelities to color-code cultivation and had an overall lower spacetime volume per $|T\rangle$ state, demonstrating the promise of surface code cultivation over color code cultivation. However, this method performs cultivation on the surface code defined on a non-orientable surface (the real projective plane, \mathbb{RP}^2) before escaping to the usual planar surface code. One significant drawback in this approach is that the non-orientable boundary conditions of \mathbb{RP}^2 mean the cultivation circuit requires many long-distance connections that are difficult to implement, even in neutral atoms. In addition, low-depth unitary injection and expansion circuits are not known for the \mathbb{RP}^2 surface code, so that state injection and intermediate code growth must be done with measurement-based circuits which require mid-circuit measurements and feedback, significantly slowing the procedure in neutral atom plat-

* jahan@logiqal.com

forms with slow measurements.

In this work, we combine ideas from \mathbb{RP}^2 cultivation with the mid-cycle trick [23, 24] to directly cultivate $|T\rangle$ states on the planar surface code. Our overall approach is motivated by the constraints of neutral atom systems: We use only two-qubit gates, we restrict our qubit movements to rigid translations of a small number of fixed arrays of qubits, and we avoid mid-circuit measurement. Sticking to these restrictions means we do not necessarily use the most effective possible circuits in terms of depths, gate counts, or error rates, but nonetheless achieve fidelities competitive with color and \mathbb{RP}^2 cultivation protocols.

We note that cultivation can be done at different distances, where increasing the distance increases the fidelity but decreases the success rate. Previous cultivation approaches were restricted to occur at odd d , since the color code cannot have even distance and the \mathbb{RP}^2 code is not fold-dual at even distance. Surface code cultivation, by contrast, can be done at any distance, allowing finer-grained trade-offs between fidelity and success rate.

II. RESULTS

We begin with an overview of our approach to cultivation and a presentation of numerical results; we explain each stage of cultivation in more detail in the next section.

Cultivating $|T\rangle$ states on the planar surface code, just as in cultivation on the color code or \mathbb{RP}^2 surface code [1, 2], proceeds in three stages:

1. Injection: We prepare a magic state in a distance-3 surface code.
2. Cultivation: We repeatedly measure the stabilizers and the logical H_{XY} operator of the code, possibly growing the code to a higher-distance during this process. Measuring H_{XY} verifies that we are in the logical $|T\rangle$ state, as this state is the $+1$ eigenstate of H_{XY} . In this stage, we postselect on any incorrect measurement outcomes, discarding the attempt.
3. Escape: We grow the surface code to a larger distance surface code that is capable of protecting the logical information to the desired fidelity. In this stage, we postselect on the complementary gap [25].

By repeatedly measuring and postselecting at increasing distances in step 2, we generate injection circuits where all errors of weight up to $(d-1)$ are flagged and can be postselected out.

We illustrate the injection/cultivation stages of our distance-3 cultivation procedure in Fig. 1. For distance-5 cultivation, we run the distance-3 cultivation, then grow the surface code from $d=3$ to $d=5$ and repeat the cultivation procedure at $d=5$. For distance-4 cultivation, we run a modified distance-3 cultivation in which we only measure the stabilizers once, then grow the surface code from $d=3$ to $d=4$ and repeat the cultivation

procedure at $d=4$ (now measuring the $d=4$ stabilizers twice). We note that, just in the case of color code cultivation, in order to actually flag all errors of weight less than $d=4$ or $d=5$, we actually need to measure the stabilizers at $d=4, 5$ more than twice; however, just as in color code cultivation, we find that only measuring the stabilizers twice results in an improved acceptance rate with negligible impact on the fidelity.

For injection, we use a unitary circuit to prepare the distance-3 magic state. Similar to Ref. [1] we design an injection circuit where the T rotation occurs midway through. This construction allows the circuit to detect single-qubit X errors and ensures the only distance-1 errors in the injection circuit are Z errors at the spacetime location of the T gate. The unitary encoding circuit allows us to avoid the mid-circuit measurement and feedback required in Ref. [2].

In the cultivation stage, we need to both measure the stabilizers and measure the logical H_{XY} operator. To measure the logical H_{XY} operator, we want to deform the surface code into a *self-dual* code where the X and Z stabilizers and logical operators exactly overlap and thus H_{XY} is transversal. Ref. [2] demonstrated that it is straightforward to deform *fold-dual* code, where the X and Z stabilizers and logical operators are related by reflection across a fold line, into a self-dual code using ancilla qubits. However, the rotated surface code is not fold-dual, so we cannot directly use this method. Fortunately, midway through the syndrome extraction circuit, the mid-cycle state of the rotated surface code is the *unrotated* surface code, which is fold-dual across the diagonal. Therefore, we choose to measure H_{XY} halfway through the syndrome extraction cycle, by deforming the mid-cycle state into a self-dual code. To deform the mid-cycle state into a self-dual code, we use a simpler method than Ref. [2], as it is easier to preserve the distance of the mid-cycle state than the \mathbb{RP}^2 code. We then optionally grow the code from $d=3$ to $d=4, 5$ using another unitary circuit, again avoiding the mid-circuit measurement and feedback in Ref. [2].

Finally, our escape state is more straightforward than either of Refs. [1, 2]; we simply grow the surface code directly into a larger surface code by initializing new qubits in $|+\rangle$ and $|0\rangle$ and measuring stabilizers of the larger code, as in any other surface code injection protocol [7, 15, 17, 35]. After measuring the larger code stabilizers several times, we can compute the complimentary gap to estimate how confident the decoder is in our result [1, 25]. By varying the cutoff for accepting the state, we trade off between the fidelity of the final magic state and the number of retries required to accept the state.

We report numerical simulations of our procedure compared to previous procedures in Fig. 2 and Table I, using a standard depolarizing error model with $p=0.001$ (see Appendix for details). To enable efficient Clifford simulations, we follow Refs. [1, 2] and replace the $|T\rangle$ state with the Clifford state $S|+\rangle$ in our simulations. As in Ref. [1], we report our error rate as double the error

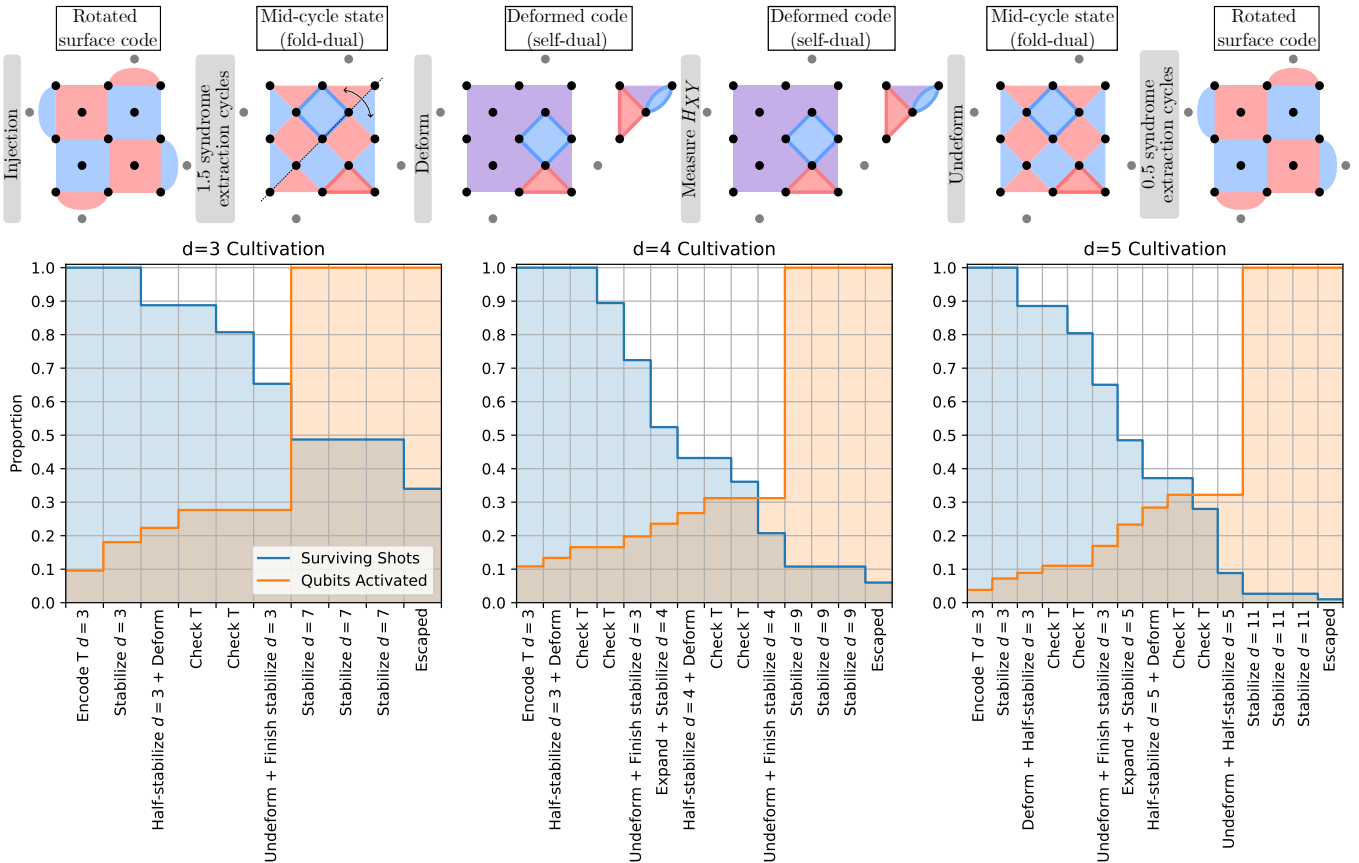


FIG. 1. Top: A sketch of distance-3 cultivation. We begin with a magic state injected into the rotated surface code. We then perform a full round of syndrome extraction, followed by another half-round of syndrome extraction to get the code into the mid-cycle state. The mid-cycle state is fold-dual across the diagonal line shown. We then use ancilla qubits and a short quantum circuit to deform the mid-cycle state to a self-dual code. Note that the deformation maps the highlighted Z (X) stabilizers of the mid-cycle state above (below) the fold to stabilizers below (above) the fold; similarly, it maps Z (X) stabilizers below (above) the fold to stabilizers above (below), making the code self-dual. We measure H_{XY} using an ancilla cat state (not shown), and reverse the deformation to return us to the mid-cycle state. We then complete the second half of the syndrome extraction cycle. From here, we can either grow the code to a higher distance and repeat the cultivation, or escape, depending on the desired fidelity of the final magic state.

Bottom: Timelines demonstrating each stage of $d = 3, 4, 5$ cultivation. We grow the code (orange) while postselecting (blue). The expected spacetime volume is given by the integral of the product of these two curves, divided by the overall success rate. Note that this estimate of the spacetime volume is somewhat arbitrary, and was chosen only to enable comparisons with color code cultivation.

rate given by the $S|+\rangle$ simulation, to roughly account for an empirically observed difference between $S|+\rangle$ and $|T\rangle$ cultivation. Compared to previous cultivation methods, our cultivation achieves lower (for $d = 3$) or similar (for $d = 5$) logical error rates than \mathbb{RP}^2 and color code cultivation, while having a discard rate and spacetime volume between that of color and \mathbb{RP}^2 cultivation. In addition, our $d = 4$ cultivation has a fidelity surprisingly close to $d = 5$ cultivation at much lower discard rates. Due to limited computational resources, we do not simulate $d = 6$ cultivation, but we expect $d = 6$ surface code cultivation to be a much more feasible route to cultivate states with fidelity $< 10^{-10}$ than $d = 7$ color or \mathbb{RP}^2 cultivation. Our simulations are all performed with three rounds of error correction at the final distance before computing

the complementary gap; we have tested that our results do not notably change when instead using five rounds of error correction, indicating both that we are not leaving potential gap information on the table by using too few error correction rounds at the final distance, and that our final distances are sufficiently large to protect our logical states to the desired fidelity with a negligible amount of postselection.

We also include numerical simulations of our cultivation circuits under a modified depolarizing error model without idle errors, which may be relevant for neutral atom qubits with extremely long idle times. In this error model, we can establish that the ungrown logical error rates (before the escape stage) are 2 to 3 orders of magnitude lower, and the ungrown discard rates are a fac-

	Cultivation protocol	Noise model	Error rate (ungrown)	Discard rate (ungrown)	Error rate (end-to-end)	Discard rate (end-to-end)	Final distance	Spacetime volume (qubit cycles)
Prev work	$d = 3$ color [1]	Uniform depolarizing	$6 \cdot 10^{-7}$	35%	$3 \cdot 10^{-6}$	80%	15	8100
	$d = 5$ color [1]		$6 \cdot 10^{-10}$	85%	$2 \cdot 10^{-9}$	99%	15	57000
	$d = 3$ \mathbb{RP}^2 [2]		$2 \cdot 10^{-6}$	49%	$3 \cdot 10^{-6}$	58%	7	900
	$d = 5$ \mathbb{RP}^2 [2]		$7 \cdot 10^{-10}$	91%	$2 \cdot 10^{-9}$	93%	11	6200
This work	$d = 3$ surface	Uniform depolarizing	$1 \cdot 10^{-6}$	54%	$1 \cdot 10^{-6}$	66%	7	900
	$d = 4$ surface		$9 \cdot 10^{-9}$	90%	$1 \cdot 10^{-8}$	94%	9	4400
	$d = 5$ surface		$1 \cdot 10^{-9}$	98%	$2 \cdot 10^{-9}$	99%	11	24600
This work	$d = 3$ surface	Uniform depolarizing	$4 \cdot 10^{-8}$	17%	$9 \cdot 10^{-8}$	33%	7	650
	$d = 4$ surface	Uniform depolarizing	$2 \cdot 10^{-11}$	39%	-	-	-	-
	$d = 5$ surface	without idle	$5 \cdot 10^{-12}$	54%	-	-	-	-

TABLE I. Comparison of error rates, discard rates, and spacetime volumes for previous cultivation protocols versus this work, for a physical depolarizing error rate $p = 10^{-3}$. The ungrown error rates (without escape) were estimated by enumerating all logical errors up to distance 5. Note that [1] reported the error rate as double the simulated $S|+$ cultivation error rate, to account for the difference between cultivating $|T\rangle$ and $S|+$, while [2] reported the error rate as the simulated $S|+$ error rate (so the reported error rates in [2] are smaller than [1] by a factor of two). We have made all numbers in this chart consist with the doubling convention of [1].

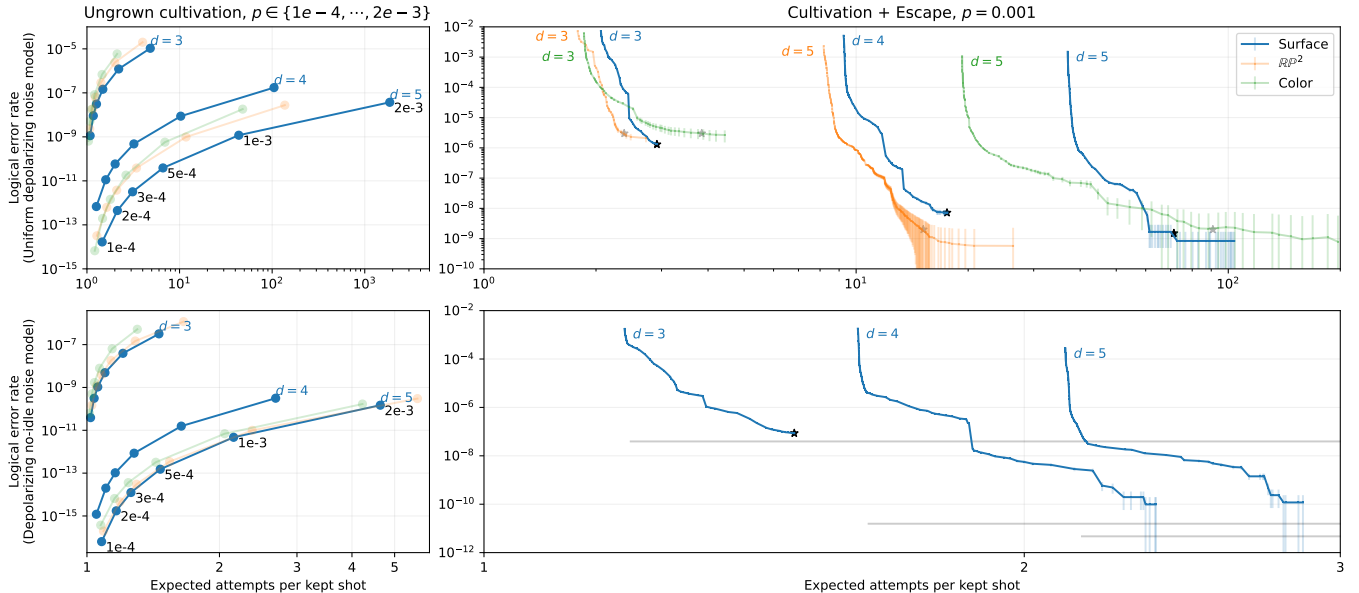


FIG. 2. The error and discard rates of surface code cultivation, compared to previous work on color [1] and \mathbb{RP}^2 [2] cultivation. We plot two different error models, the uniform depolarizing model studied in [1, 2] (top row) and a depolarizing model with idle errors removed relevant to neutral atom qubits (bottom row). The left column shows the error/discard rates for cultivation without escape for various values of the physical error rate p , estimated by enumerating all errors of weight ≤ 5 ; the right column shows the error/discard rates of cultivation plus escape for $p = 0.001$, estimated using STIM [26] and PyMatching [27]. Stars in the right column denote the points used for Table I.

Note that the results in the bottom right are not directly comparable with previous work, as previous cultivation protocols did not provide simulation results for this error model. The $d = 4, 5$ simulations establish we can reach a 10^{-10} error rate at fairly low discard rate, but we do not have sufficient data to determine whether a higher gap cutoff could result in even lower error rates. The horizontal lines in the bottom right figure represent the ungrown logical error rates taken from the bottom left figure, which serves as a lower bound for the achievable logical error rate.

For all panels, we double the simulated error rate as in [1].

tor of 2 to 3 lower. However, establishing the error and discard rates of cultivation plus escape is prohibitively expensive for $d = 4, 5$. We note that for previous simulations, the escape stage approximately doubles or triples the error rate, so we may conjecture that the $d = 4, 5$

surface codes still maintain errors $\sim 10^{-11}$ under this error model; however, our simulations can only establish error rates of $< 10^{-10}$. When comparing to color or \mathbb{RP}^2 cultivation, we do not have simulations of cultivation plus escape, as previous work did not consider

this error model. However, we note that unlike in the case of the uniform depolarizing error model, the performance of all three ungrown $d = 5$ cultivation circuits are quite similar, suggesting that $d = 5$ surface code cultivation may match \mathbb{RP}^2 cultivation under this error model. While we do not highlight these numbers in our table, as they are not relevant to the comparison with prior work, it suggests that the performance of cultivation on a given platform is highly sensitive to the details of the error model.

We end with two notes of caution on comparing the results of this paper to previous cultivation protocols. First, the spacetime volume figures in Fig. 1 and Tab. I should not be taken too seriously. Our division of our circuit into “cycles” is fairly arbitrary, and done only to allow for rough comparison to previous work. Notably, our circuit contains operations like code deformation that do not exist in the color code cultivation circuit. In addition, the number of active qubits (the orange curve in Fig. 1) depends on how we choose to rearrange and recycle qubits. Finally, we note that spacetime volume computed via the blue curves in 1 assumes that we pause after every cycle to complete the measurement before deciding whether to continue the cultivation attempt; this was also assumed for the \mathbb{RP}^2 spacetime volume in Ref. [2]. However, for neutral atoms qubits with slow measurements, it may be more efficient to batch measurements. Indeed, one virtue of our approach over Ref. [2] is that no part of our circuit requires feed-forward from a previous measurement outcome, meaning we do not need to be slowed down by slow measurement times. We thus caution that the spacetime volume is not necessarily a meaningful metric of comparison, and more hardware-specific measures will be needed in the future.

Second, we note that both the uniform depolarizing and the depolarizing no-idle error models likely do not capture the relevant features of neutral atom qubits. A more accurate error model would include noise induced by qubit movement and transfers between traps, in which the relative performance of the \mathbb{RP}^2 circuits would likely degrade but the performance of the color circuits may improve somewhat. These simulations also do not account for qubit leakage, which becomes increasingly damaging as the circuit depth increases. On the other hand, we also do not currently take advantage of the structure of noise available in certain in neutral atoms, such as erasure bias [28? ? -30], which may improve performance [31, 38]. As a rough approximation, if a fraction R_e of errors are erasures, the leading order error rate of the ungrown patch will go from Cp^d to $C((1 - R_e)p)^d$ for some constant C , meaning that a realistic 90% erasure fraction [28] could improve the logical error rate of $d = 5$ cultivation by a factor of 10^5 (see also [38]).

III. CONSTRUCTING THE CULTIVATION CIRCUIT

We begin by noting that $|T\rangle$ is the unique $+1$ eigenstate of the operator $H_{XY} := (X + Y)/\sqrt{2}$. Our goal is to inject $|T\rangle$ with as high a fidelity as possible, then alternate measuring the stabilizers with fault-tolerantly measuring the logical H_{XY} operator to ensure we have successfully prepared the $|T\rangle$ state. We can do this measurement repeatedly at increasing code distances, if desired. Measuring H_{XY} is the primary challenge, since the surface code does not posses a transversal H_{XY} gate.

A. Injection and code growth

Following [1], we use a unitary injection circuit to prepare the $|T\rangle$ state, adapted from the unitary injection circuit for $|0\rangle$ and $|+\rangle$ given in [32]. Our circuit is illustrated in Fig. 3. This circuit detects all distance-1 X errors, and the only undetectable distance-1 Z errors are those at the spacetime location of the T gate. This is similar to the injection circuit in Ref. [1] which is similarly protected against distance-1 errors, and stands in contrast to the measurement-based \mathbb{RP}^2 injection circuit in Ref. [2] which has a greater number of distance-1 errors (for example, the \mathbb{RP}^2 circuit is exposed to single-qubit errors at initialization). In addition, the measurement-based \mathbb{RP}^2 injection circuit requires mid-circuit measurement and feedback to project the code into the $+1$ eigenstate of all stabilizers, which we avoid with our unitary initialization.

To grow a $d = 3$ surface code to a $d = 4$ or $d = 5$ surface code, we use the unitary growth circuits illustrated in Fig. 4, which are similar to the growth circuits in Ref. [33] but lower depth. Unitary growth also avoids the midcircuit measurement and feedback used to grow the $d = 3$ \mathbb{RP}^2 code to a $d = 5$ \mathbb{RP}^2 code in Ref. [2].

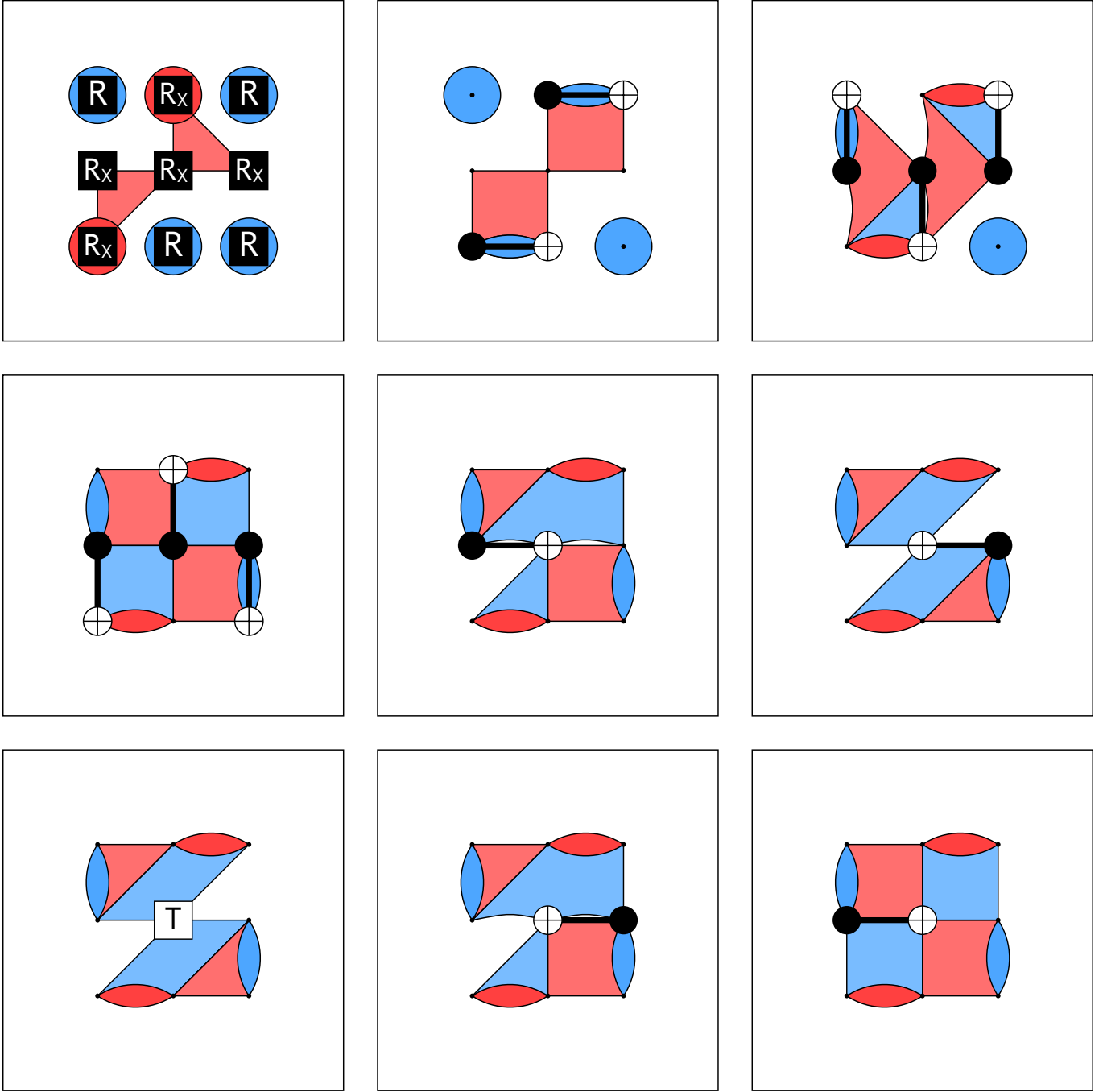


FIG. 3. The unitary circuit we use to inject a magic state into the surface code, adapted from similar circuits in [32]. We illustrate the eight initial stabilizers that evolve to be the stabilizers of the $d = 3$ surface code. The logical X operator begins as a single physical X on the center qubit (not shown). This means that at initialization, a single-qubit error flipping the X logical operator would also flip the two triangular X stabilizers, making this error detectable. Furthermore, the T rotation occurs with two Z stabilizers touching it, meaning that any single-qubit X or Y error at this location is detectable. Overall, the only undetectable single-qubit errors in this circuit are Z errors at the spacetime location of the T gate.

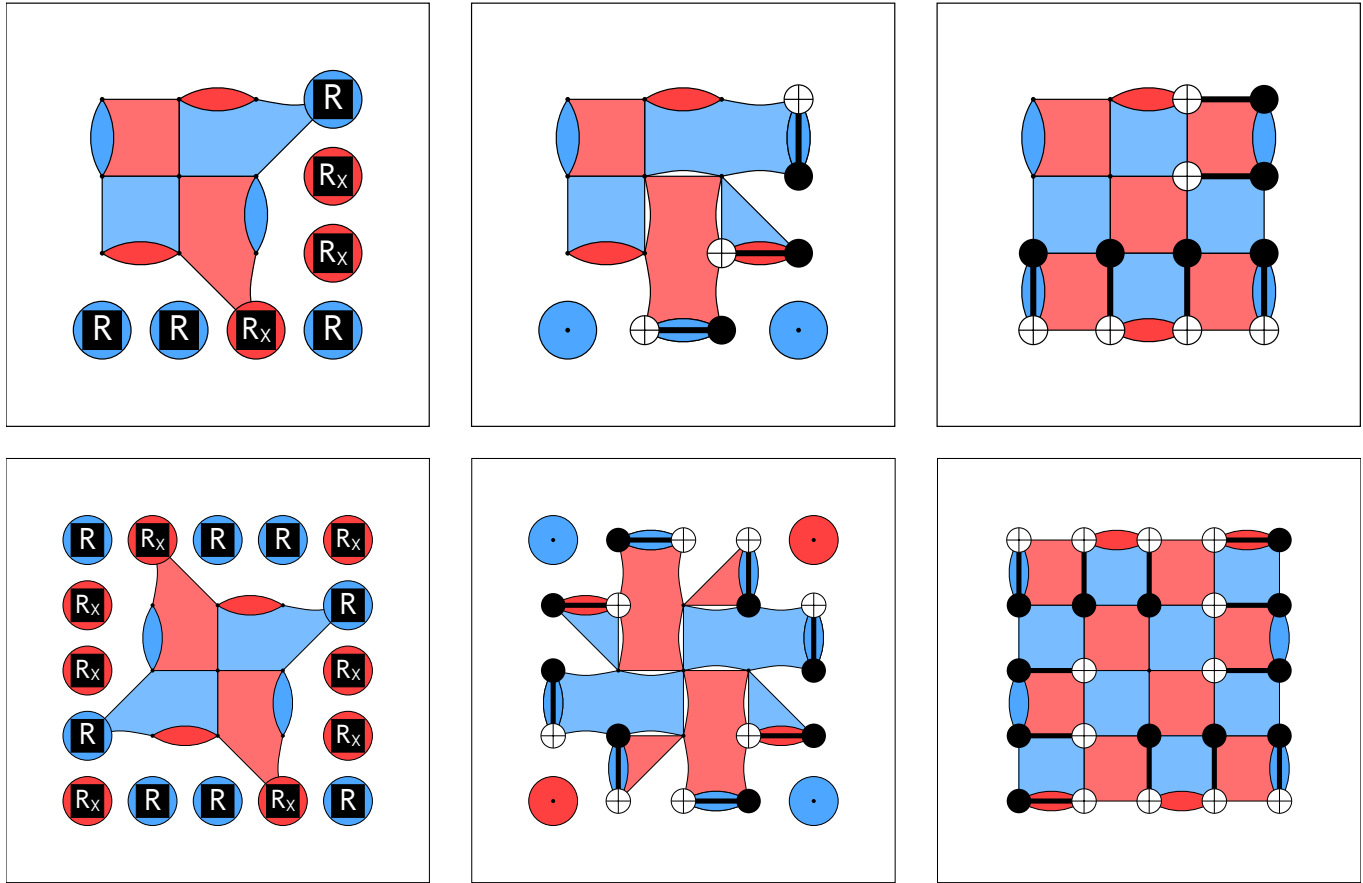


FIG. 4. Unitary circuits to grow the surface code from $d = 3$ to $d = 4$ (top) or $d = 5$ (bottom).

B. Measuring logical H_{XY}

We will see below that it is relatively straightforward to fault-tolerantly measure the logical H_{XY} operator in codes that admit a transversal H_{XY} gate [1, 10, 11]. The surface code does not admit a transversal H_{XY} gates, but self-dual codes do. In the same spirit as Ref. [2], we will deform our surface code into a self-dual code in order to measure the logical H_{XY} operator.

1. Transversal H_{XY} on self-dual codes

It has long been known that the logical operators H_{XY} and $iZH_{XY} = (X - Y)/\sqrt{2}$ can be implemented transversally in *self-dual* CSS codes [12, 34], where each $\otimes Z_i$ stabilizer is in one-to-one correspondence with a dual $\otimes X_i$ stabilizer supported on the same qubits (and the same for a basis of logical operators). Given a self-dual basis of logical operators, each operator is necessarily supported on an odd number of qubits ($2w + 1$), where in codes with multiple logical operators w can depend on the particular logical operator. We claim that a transversal H_{XY} gate applied to all the physical qubits applies a logical H_{XY} to logical qubits with w even or a logical $iZH_{XY} = (X - Y)/\sqrt{2}$ to logical qubits with w odd. Conversely, a transversal iZH_{XY} applies a logical iZH_{XY} to logical qubits with w even and a logical H_{XY} to logical qubits with w odd.

To demonstrate this claim, we first note that in the Heisenberg picture H_{XY} sends $X \leftrightarrow Y$ and $Z \rightarrow -Z$. Similarly, iZH_{XY} sends $X \leftrightarrow -Y$ and $Z \rightarrow -Z$. Thus, we need to show that the transversal H_{XY} maps each set of self-dual logical Pauli operators as $X_L \leftrightarrow (-1)^w Y_L$ and $Z_L \rightarrow -Z_L$, while preserving each stabilizer.

We begin with the logical operators. Z_L is given by a product of $(2w + 1)$ physical Z operators, $Z_L = \otimes^{2w+1} Z_i$. Since each physical Z_i operator is sent to $-Z_i$ by transversal H_{XY} , Z_L is sent to $(-1)^{2w+1} Z_L = -Z_L$. As for X_L and Y_L , we note that $Y_L = iX_L Z_L = (-1)^w \otimes^{2w+1} Y_i$, so H_{XY} sends $X_L \rightarrow \otimes^{2w+1} Y_i = (-1)^w Y_L$ and $Y_L \rightarrow (-1)^w \otimes^{2w+1} X_i = (-1)^w X_L$. Thus, for logicals with even w (i.e., distance 5, 9, 13, ...) the transversal H_{XY} acts as a logical H_{XY} , while for logicals with odd w (i.e., distance 3, 7, 11, ...) it acts as a logical iZH_{XY} .

We now turn to the stabilizers. In any self-dual code, every stabilizer has even weight. If we apply a transversal H_{XY} operator to each qubit, it will send a $2w$ -qubit stabilizer $\otimes^{2w} Z_i \rightarrow (-1)^{2w} \otimes^{2w} Z_i = \otimes^{2w} Z_i$. It will also send a $2w$ -qubit stabilizer $\otimes^{2w} X_i$ to $(-1)^w \otimes^{2w} X_i \otimes^{2w} Z_i$, which is equal to $\otimes^{2w} X_i$ provided that we are in the $(-1)^w$ eigenstate of the Z stabilizer. In other words, transversal H_{XY} preserves the stabilizers, provided we are in a code state where each singly-even Z stabilizer (weight 2, 6, 10, etc) is (-1) and each doubly-even stabilizer (weight 4, 8, 12, etc) is $(+1)$. As long as our stabilizers have been initialized in a known value, we can ensure the Z

stabilizers have the appropriate value by applying a layer of Pauli X operators; we can also ensure that the stabilizers have the appropriate values by initializing some qubits in $|1\rangle$ rather than $|0\rangle$ in the injection and growth steps. Note that the fact that we need the Z stabilizers to have certain values is why we prefer unitary initialization circuits, rather than measurement-based initialization circuits which project stabilizers into random values that are not known until after measurement.

We can similarly show that a transversal iZH_{XY} operator acts as a logical iZH_{XY} on logicals with w even and a logical H_{XY} on logicals with w odd, with the same requirement on the value of the Z stabilizers.

2. Deforming to self-dual

To measure the logical H_{XY} operator, we want to deform the rotated surface code into a self-dual code with a short quantum circuit. To develop our deformation circuit, we use two facts. First, it was pointed out in Ref. [2] that starting from a *fold-dual* code, in which there exists some fold line such that each $\otimes X_i$ stabilizer is in one-to-one-correspondence with a $\otimes Z_i$ stabilizer across the fold (and the same for a basis of logical operators), it is relatively simple to deform into a self-dual code. Second, it is known that halfway through the syndrome extraction cycle of the rotated surface code, the mid-cycle state of the unrotated surface code plus its ancilla measurement qubits is the state of the unrotated surface code [23, 24], which is fold-dual across the diagonal line (see Fig. 5). Overall, then, our strategy is to first transform the unrotated surface code into a fold-dual code at no cost (since we need to measure the stabilizers anyway), and then use a short quantum circuit to deform the fold-dual mid-cycle state into a self-dual code.

Our deformation circuit should take each single-qubit X operator and its fold-dual Z partner to overlapping $\otimes X$ and $\otimes Z$ operators. This is not possible do to without ancilla qubits; however, with a single ancilla for each pair of fold-dual qubits, we can arrange for the X and Z operators to overlap. We illustrate our circuit for $d = 3$ in Fig. 6. Each pair of fold-dual qubits has a single ancilla qubit associated with it, and we have arranged the ancilla qubits into a triangular patch next to the surface code. Our circuit takes X operators above the fold and Z operators below the fold to XX/ZZ operators on the qubit above the fold and the matching qubit on the triangular ancilla patch. Similarly, it takes Z operators above the fold and X operators below the fold to ZZ/XX operators on the qubit below the fold and the matching qubit on the triangular ancilla patch. The result is that all X and Z stabilizers (and the X and Z logical operator of the surface code) are now overlapping and the code is thus self-dual. In terms of the distance d of the surface code, the logical operators have weight $(2d - 1)$, so that for odd d the logical H_{XY} is given by transversal H_{XY} , while for even d it is given by transversal iZH_{XY} .

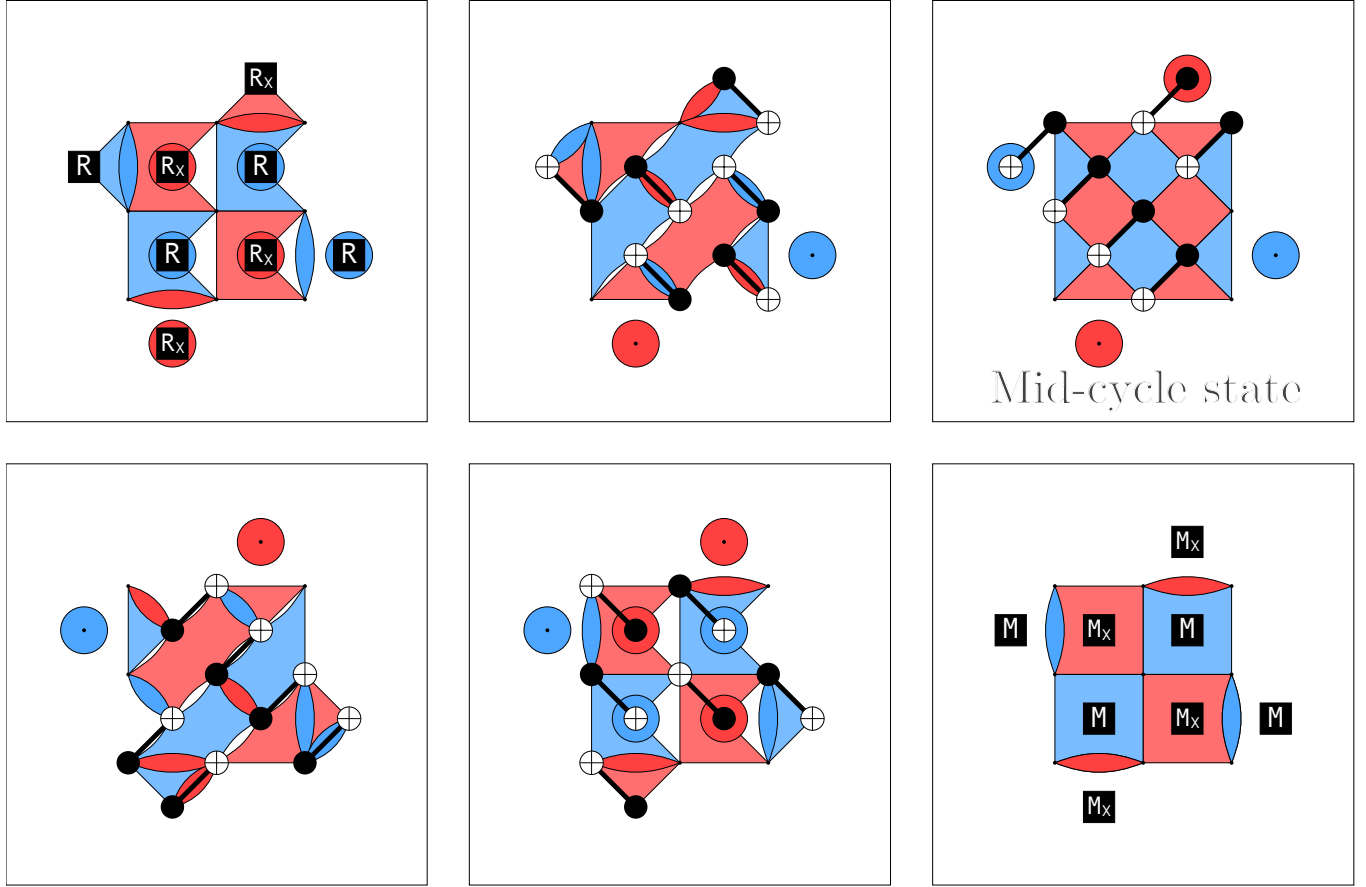


FIG. 5. The evolution of stabilizers of a rotated surface code over a syndrome extraction cycle. We see that in the mid-cycle state, the stabilizers evolve to the stabilizers of the unrotated surface code, with the outer ancillas in product states [23, 24]. Ignoring the trivial outer ancillas, the mid-cycle state is fold-dual across either diagonal line.

Note that the ancilla qubits introduce their own self-dual logical operators, since we have increased the number of qubits in the code but not increased the number of stabilizers. These additional logical operators must be initialized in a state that is invariant under the transversal H_{XY}/iZH_{XY} operator, in order for this transversal operator to only act on the logical surface code degree of freedom. Each self-dual ancilla logical operator has weight three, so the transversal H_{XY}/iZH_{XY} operator acts as a logical iZH_{XY}/H_{XY} operator on these logical qubits. To ensure these degrees of freedom are invariant, we initialize the ancilla qubits in $|T\rangle$ ($T^\dagger|+\rangle$) for d even (odd), which is the $(+1)$ eigenstate of H_{XY} (iZH_{XY}). Note that initializing the physical ancilla qubit in $T^\dagger|+\rangle$ is no more difficult than initializing them in any other state.

Compared to Ref. [2], our deformation circuit is considerably simplified. Ref. [2] took pairs of fold-dual qubits (or pairs of pairs) and concatenated them into a $[[4, 2, 2]]$ (or $[[6, 4, 2]]$) error-detecting code. Essentially, they ensured that the fold-dual X and Z operators were sent to overlapping XX and ZZ operators, but also introduced additional self-dual $XXXX$ and $ZZZZ$ stabiliz-

ers rather than introducing additional invariant logical degrees of freedom. They required these extra stabilizers in order to maintain the code distance, as pairing fold-dual qubits in the \mathbb{RP}^2 code without these additional stabilizers halves the code distance. However, pairing fold-dual qubits in the unrotated surface code does not affect the distance [24], thus we do not need to introduce additional stabilizers and may use only one ancilla qubit per fold-dual pair and a simpler deformation circuit.

3. Measuring logical H_{XY} with a cat ancilla

Once the code has been deformed into a self-dual code, we can measure the logical H_{XY} operator using a cat state ancilla and controlled- H_{XY} gates, as in Refs. [1, 2, 10, 11]. Our particular circuit is a “double-checking” circuit, as in Ref. [1, 2] in which the circuit is run in one direction to measure the logical operator, and then run in reverse to measure a set of flag qubits that detect errors during the forward measurement. We illustrate the forward half of our double-checking circuit for $d = 5$ in Fig. 7. For odd d we want to apply a

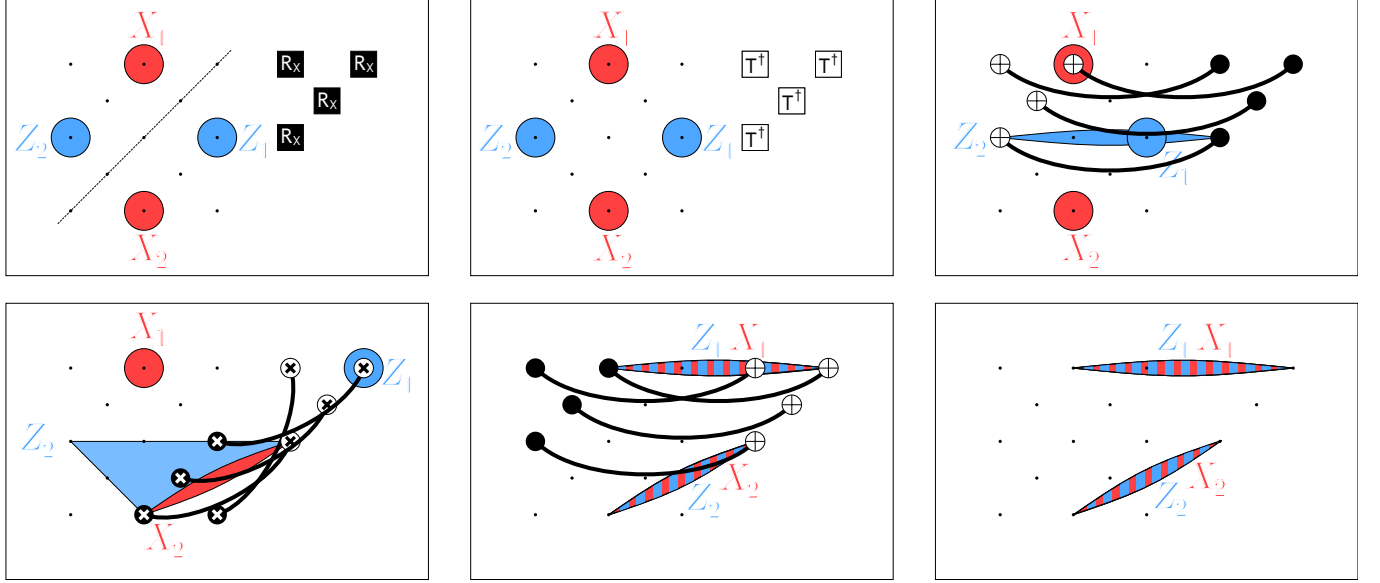


FIG. 6. The deformation circuit takes us from the unrotated surface code to a self-dual code with a transversal H_{XY} . The gate denoted by black/white circles with \times s at the center is the CXSWAP gate which is equivalent to pair of CX gates, the first with the control on the white circle and the second with the control on the black circle. We illustrate two pairs of X and Z operators that are related by reflection across the fold. Our circuit takes X operators above the fold and Z operators below the fold to XX/ZZ operators on the qubit above the fold and the matching qubit on the triangular ancilla patch. Similarly, it takes Z operators above the fold and X operators below the fold to ZZ/XX operators on the qubit below the fold and the matching qubit on the triangular ancilla patch. The ancilla qubits are initialized in $T^\dagger|+\rangle$, making the logical degrees of freedom introduced by the ancilla qubits invariant under transversal H_{XY} . To undo the deformation, we run the circuit in reverse and measure the triangular ancilla patch in the X basis.

controlled- H_{XY} gate between the ancilla and the code. We convert this to a controlled- X gate by applying a layer of T^\dagger gates, because $T^\dagger H_{XY} T = X$. For even d , we instead apply a controlled- iZH_{XY} gate, which we convert to controlled- X gates by applying a layer of T gates, since $T(iZH_{XY})T^\dagger = X$.

4. Reversing the deformation

After measuring H_{XY} , we reverse the deformation circuit and measure the triangular patch of ancillas in the X basis to return to the mid-cycle state, and complete the syndrome extraction cycle to return to the rotated surface code state. If the measurement of the triangular patch of ancilla qubits don't all return $(+1)$, or the final syndrome measurements don't return the correct values, we discard the attempt.

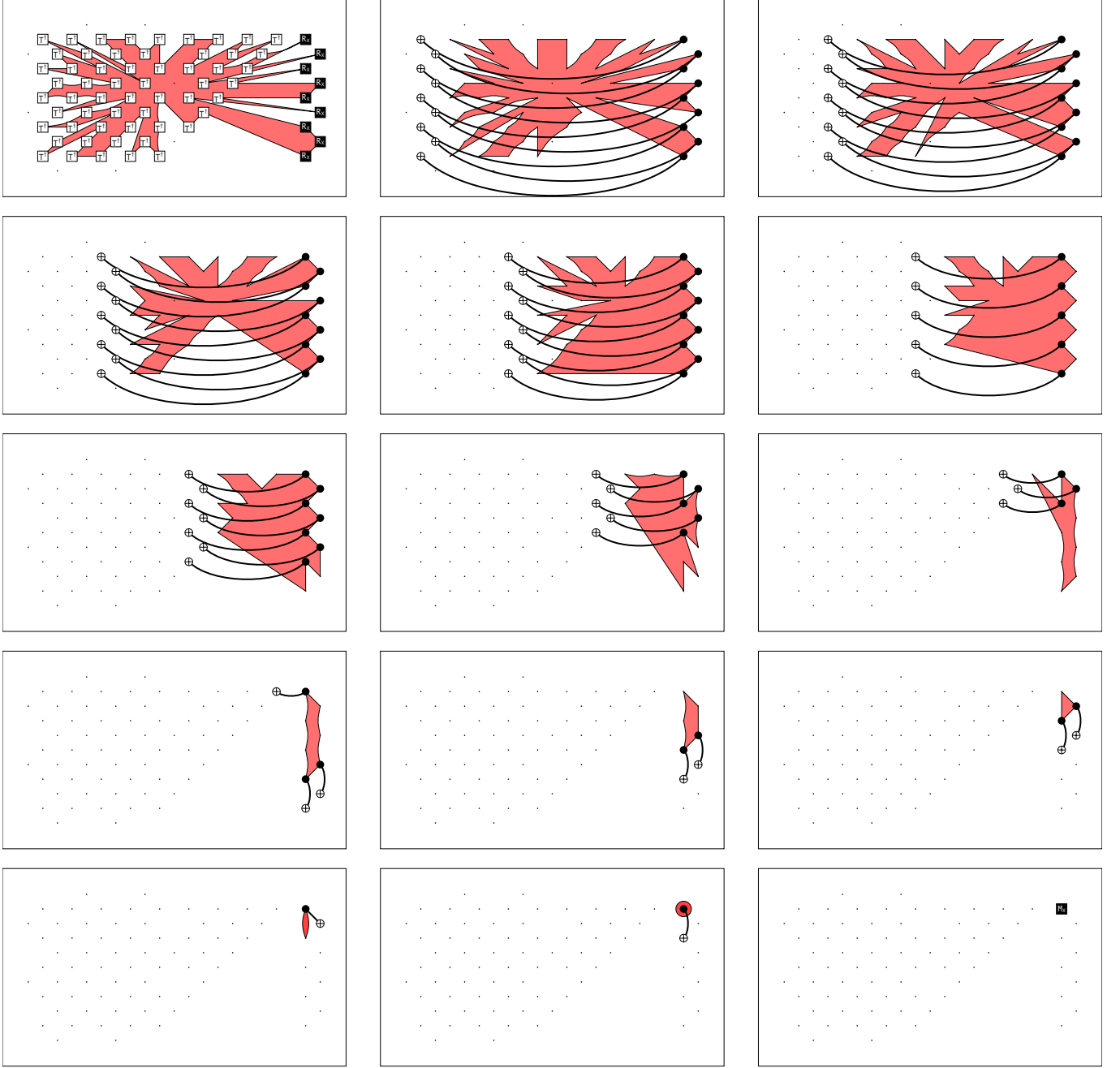


FIG. 7. The first half of our double-checking circuit for measuring transversal H_{XY} . We begin by applying a layer of T^\dagger gates to the code qubits, to transform the problem into measuring transversal X , and initializing a column of ancillas in $|+\rangle$ which will perform the measurement. The large $\otimes X$ operator we are measuring is tracked throughout the circuit. To shrink this operator to a single qubit, we move the column of ancilla qubits across the data qubits, applying CX gates between the ancilla and code qubits at each step, followed by CX gates among the ancilla qubits. Once the operator is supported on a single qubit, we measure that qubit. To complete the double-checking, we run the circuit in reverse and measure each qubit in the ancilla column in the X basis. In the absence of errors, all measurements should be $+1$.

C. Escape

Our escape stage is simple: We initialize new qubits in $|+\rangle$ and $|0\rangle$ according to standard surface code growth protocols [7, 15, 17, 35], and measure the stabilizers of the larger code several times. We then compute the complementary gap [1, 25] just as in color code cultivation in order to estimate how confident the decoder is in our result. We can postselect on this complementary gap to trade off between the fidelity of the final magic state and the number of retries required to accept the state.

Note that the most straightforward implementation for computing the complementary gap requires a boundary where logical operators can terminate [25, 36]; for this reason, it is not straightforward to compute the complementary gap in \mathbb{RP}^2 cultivation. This is why Ref. [2] instead used a different measure (the “2D soft output” [37]) to estimate the decoder’s confidence, a complication we do not encounter when cultivating directly on the planar surface code.

IV. CONCLUSION

We have presented a new surface code cultivation protocol for $|T\rangle$ states that avoids the drawbacks of previous attempts at surface code cultivation. Our simulations and resource estimates show our protocol is competitive with previous color code and \mathbb{RP}^2 cultivation protocols when considering uniform depolarizing noise and measures of spacetime volume used in previous work, and likely further improves relative to previous protocols when considering a modified error model without idle errors.

In the future, it will be interesting to consider how these estimates are modified by more realistic models for neutral atom systems. On the optimistic side, the long coherence times of neutral atom qubits means that idle errors are often negligible; we can also incorporate erasure conversion [28–31], which will allow us to postselect errors more effectively [38] and will likely enable the computation of a finer-tuned complementary gap. On the other side, errors induced by qubit movement and trap transfers are not accounted for in our simulations. We also neglect the possibility of leakage, which may be significant for deep cultivation circuits. Leakage is relatively benign in postselected circuits, as it only increases the discard rate; however, if leakage reduction units are required to keep the discard rate reasonable, they may add additional gates and correspondingly increase the noise [23, 39–42].

We also re-emphasize that beyond the noise model model, the measure of spacetime volume in previous works is ad-hoc and not necessarily relevant to neutral atom qubit platforms. More accurate spacetime comparisons will require careful consideration of atom move times and measurement times.

NOTE ADDED

While completing this manuscript, we became aware of two pieces of related work by the Puri and AWS research groups, which appear in the same arXiv posting as the present work.

ACKNOWLEDGMENTS

We thank Jeff Thompson, Sebastian Horvath, and Elmer Guardado-Sanchez for helpful conversations. We thank Kaavya Sahay and Shruti Puri for discussing their related work with us, and coordinating the release of their paper. We thank Ken Brown and Jeff Thompson for suggestions and feedback on the manuscript. The code used to generate noisy STIM circuits and enumerate short-distance errors was modified from code included with [1].

APPENDIX: NOISE MODEL

Here, we specify the noise models we use in the simulations. To enable comparison with previous works, we use the same uniform depolarizing noise model of [1, 2]. The noise model consists of

- Single-qubit gates are followed by a single-qubit depolarizing channel with strength p .
- Two-qubit gates are followed by a two-qubit depolarizing channel with strength p .
- Idle qubits during single or two-qubit gates incur a single-qubit depolarizing channel with strength p .
- Initialization in $|0\rangle$ instead prepares $|1\rangle$ with probability p , and similar for $|+\rangle$.
- Measurement results are flipped with probability p .

To estimate the advantage of qubits like neutral atoms which may have very long idle coherence times, we also consider a depolarizing noise model in which the idle errors are removed.

[1] C. Gidney, N. Shutty, and C. Jones, [Magic state cultivation: Growing T states as cheap as CNOT gates](#) (2024), arXiv:2409.17595 [quant-ph].

[2] Z.-H. Chen, M.-C. Chen, C.-Y. Lu, and J.-W. Pan, [Efficient magic state cultivation on \$\mathbb{RP}^2\$](#) (2025), arXiv:2503.18657 [quant-ph].

[3] D. Gottesman and I. L. Chuang, Quantum teleportation is a universal computational primitive, *Nature* **402**, 390 (1999), arXiv:quant-ph/9908010.

[4] S. Bravyi and A. Kitaev, Universal quantum computation with ideal clifford gates and noisy ancillas, *Physical Review A* **71**, 022316 (2005), arXiv:quant-ph/0403025.

[5] S. Bravyi and R. König, Classification of topologically protected gates for local stabilizer codes, *Physical Review Letters* **110**, 170503 (2013).

[6] F. Pastawski and B. Yoshida, Fault-tolerant logical gates in quantum error-correcting codes, *Physical Review A* **91**, 012305 (2015).

[7] Y. Li, A magic state's fidelity can be superior to the operations that created it, *New Journal of Physics* **17**, 023037 (2015), arXiv:1410.7808 [quant-ph].

[8] S. Bravyi and J. Haah, Magic state distillation with low overhead, *Physical Review A* **86**, 052329 (2012), arXiv:1209.2426 [quant-ph].

[9] D. Litinski, Magic state distillation: Not as costly as you think, *Quantum* **3**, 205 (2019), arXiv:1905.06903 [quant-ph].

[10] T. Itogawa, Y. Takada, Y. Hirano, and K. Fujii, Even more efficient magic state distillation by zero-level distillation (2024), arXiv:2403.03991 [quant-ph].

[11] C. Chamberland and K. Noh, Very low overhead fault-tolerant magic state preparation using redundant ancilla encoding and flag qubits, *npj Quantum Information* **6**, 1 (2020).

[12] H. Bombin and M. A. Martin-Delgado, Topological quantum distillation, *Physical Review Letters* **97**, 180501 (2006), arXiv:quant-ph/0605138.

[13] g.-i. family=Kitaev, given=A. Yu., Quantum error correction with imperfect gates, in *Quantum Communication, Computing, and Measurement*, edited by O. Hirota, A. S. Holevo, and C. M. Caves (Springer US) pp. 181–188.

[14] S. B. Bravyi and A. Y. Kitaev, Quantum codes on a lattice with boundary, quant-ph/9811052.

[15] D. Litinski, A game of surface codes: Large-scale quantum computing with lattice surgery, *Quantum* **3**, 128 (2019), arXiv:1808.02892 [quant-ph].

[16] A. G. Fowler and C. Gidney, Low overhead quantum computation using lattice surgery (2019), arXiv:1808.06709 [quant-ph].

[17] A. G. Fowler, M. Mariantoni, J. M. Martinis, and A. N. Cleland, Surface codes: Towards practical large-scale quantum computation, *Physical Review A* **86**, 10.1103/physreva.86.032324 (2012).

[18] C. Gidney and M. Ekera, How to factor 2048 bit rsa integers in 8 hours using 20 million noisy qubits, *Quantum* **5**, 433 (2021), arXiv:1905.09749 [quant-ph].

[19] E. Dennis, A. Kitaev, A. Landahl, and J. Preskill, Topological quantum memory, *Journal of Mathematical Physics* **43**, 4452, quant-ph/0110143.

[20] Y. Vaknin, S. Jacoby, A. Grimsmo, and A. Retzker, Magic state cultivation on the surface code (2025), arXiv:2502.01743 [quant-ph].

[21] E. Dennis, Toward fault-tolerant quantum computation without concatenation, *Physical Review A* **63**, 052314 (2001).

[22] R. S. Gupta, N. Sundaresan, T. Alexander, C. J. Wood, S. T. Merkel, M. B. Healy, M. Hillenbrand, T. Jochym-O'Connor, J. R. Wootton, T. J. Yoder, *et al.*, Encoding a magic state with beyond break-even fidelity, *Nature* **625**, 259 (2024).

[23] M. McEwen, D. Bacon, and C. Gidney, Relaxing hardware requirements for surface code circuits using time-dynamics, *Quantum* **7**, 1172 (2023).

[24] Z.-H. Chen, M.-C. Chen, C.-Y. Lu, and J.-W. Pan, Transversal logical clifford gates on rotated surface codes with reconfigurable neutral atom arrays (2024), arXiv:2412.01391 [quant-ph].

[25] C. Gidney, M. Newman, P. Brooks, and C. Jones, Yoked surface codes (2023), arXiv:2312.04522 [quant-ph].

[26] C. Gidney, Stim: A fast stabilizer circuit simulator, *Quantum* **5**, 497 (2021), arXiv:2103.02202 [quant-ph].

[27] O. Higgott, Pymatching: A python package for decoding quantum codes with minimum-weight perfect matching (2021), arXiv:2105.13082 [quant-ph].

[28] Y. Wu, S. Kolkowitz, S. Puri, and J. D. Thompson, Erasure conversion for fault-tolerant quantum computing in alkaline earth rydberg atom arrays, *Nature Communications* **13**, 4657 (2022).

[29] K. Sahay, J. Jin, J. Claes, J. D. Thompson, and S. Puri, High-threshold codes for neutral-atom qubits with biased erasure errors, *Physical Review X* **13**, 041013 (2023).

[30] S. Ma, G. Liu, P. Peng, B. Zhang, S. Jandura, J. Claes, A. P. Burgers, G. Pupillo, S. Puri, and J. D. Thompson, High-fidelity gates and mid-circuit erasure conversion in an atomic qubit, *Nature* **622**, 279 (2023).

[31] B. Zhang, G. Liu, G. Bornet, S. P. Horvath, P. Peng, S. Ma, S. Huang, S. Puri, and J. D. Thompson, Leveraging erasure errors in logical qubits with metastable \$^{171}\text{Yb}\$ atoms (2025), arXiv:2506.13724 [quant-ph].

[32] K. J. Satzinger, Y. Liu, A. Smith, C. Knapp, M. Newman, C. Jones, Z. Chen, C. Quintana, X. Mi, A. Dunsworth, C. Gidney, I. Aleiner, F. Arute, K. Arya, J. Atalaya, R. Babbush, J. C. Bardin, R. Barends, J. Basso, A. Bengtsson, A. Bilmes, M. Broughton, B. B. Buckley, D. A. Buell, B. Burkett, N. Bushnell, B. Chiaro, R. Collins, W. Courtney, S. Demura, A. R. Derk, D. Eppens, C. Erickson, E. Farhi, L. Foar, A. G. Fowler, B. Foxen, M. Giustina, A. Greene, J. A. Gross, M. P. Harrigan, S. D. Harrington, J. Hilton, S. Hong, T. Huang, W. J. Huggins, L. B. Ioffe, S. V. Isakov, E. Jeffrey, Z. Jiang, D. Kafri, K. Kechedzhi, T. Khattar, S. Kim, P. V. Klimov, A. N. Korotkov, F. Kostritsa, D. Landhuis, P. Laptev, A. Locharla, E. Lucero, O. Martin, J. R. McClean, M. McEwen, K. C. Miao, M. Mohseni, S. Montazeri, W. Mruczkiewicz, J. Mutus, O. Naaman, M. Neeley, C. Neill, M. Y. Niu, T. E. O'Brien, A. Opremcak, B. Pató, A. Petukhov, N. C. Rubin, D. Sank, V. Shvarts, D. Strain, M. Szalay, B. Villalonga, T. C. White, Z. Yao, P. Yeh, J. Yoo, A. Zalcman, H. Neven, S. Boixo, A. Megrant, Y. Chen, J. Kelly, V. Smelyanskiy, A. Kitaev, M. Knap, F. Pollmann, and P. Roushan, Realizing topologically ordered states on a quantum processor, *Science* **374**, 1237 (2021), arXiv:2104.01180 [quant-ph].

[33] O. Higgott, M. Wilson, J. Hefford, J. Dborin, F. Hanif, S. Burton, and D. E. Browne, Optimal local unitary encoding circuits for the surface code, *Quantum* **5**, 517 (2021), arXiv:2002.00362 [quant-ph].

[34] A. Kubica and M. E. Beverland, Universal transversal gates with color codes: A simplified approach, *Physical Review A* **91**, 032330 (2015).

[35] D. Horsman, A. G. Fowler, S. Devitt, and R. Van Meter, Surface code quantum computing by lattice surgery, New

Journal of Physics **14**, 123011 (2012).

[36] C. Gidney, [Answer to "how to force pymatching into the opposite equivalence class"](#) (2024).

[37] N. Meister, C. A. Pattison, and J. Preskill, [Efficient soft-output decoders for the surface code](#) (2024), [arXiv:2405.07433 \[quant-ph\]](#).

[38] S. Jacoby, Y. Vaknin, A. Retzker, and A. L. Grimsmo, [Magic state injection with erasure qubits](#) (2025), [arXiv:2504.02935 \[quant-ph\]](#).

[39] M. Suchara, A. W. Cross, and J. M. Gambetta, Leakage suppression in the toric code, *Quantum Info. Comput.* **15**, 997 (2015).

[40] A. G. Fowler, Coping with qubit leakage in topological codes, *Physical Review A* **88**, 042308 (2013).

[41] M. N. H. Chow, V. Buchemavari, S. Omanakuttan, B. J. Little, S. Pandey, I. H. Deutsch, and Y.-Y. Jau, Circuit-based leakage-to-erasure conversion in a neutral-atom quantum processor, *PRX Quantum* **5**, 040343 (2024).

[42] G. Baranes, M. Cain, J. P. B. Ataides, D. Bluvstein, J. Sinclair, V. Vuletic, H. Zhou, and M. D. Lukin, [Leveraging atom loss errors in fault tolerant quantum algorithms](#) (2025), [arXiv:2502.20558 \[quant-ph\]](#).